MMIF-AMIN: Adaptive Loss-Driven Multi-Scale Invertible Dense Network for Multimodal Medical Image Fusion

Tao Luo, Weihua Xu*

College of Artificial Intelligence, Southwest University, Chongqing, 400715, P.R. China

Abstract

Multimodal medical image fusion (MMIF) aims to integrate images from different modalities to produce a comprehensive image that enhances medical diagnosis by accurately depicting organ structures, tissue textures, and metabolic information. Capturing both the unique and complementary information across multiple modalities simultaneously is a key research challenge in MMIF. To address this challenge, this paper proposes a novel image fusion method, MMIF-AMIN, which features a new architecture that can effectively extract these unique and complementary features. Specifically, an Invertible Dense Network (IDN) is employed for lossless feature extraction from individual modalities. To extract complementary information between modalities, a Multi-scale Complementary Feature Extraction Module (MCFEM) is designed, which incorporates a hybrid attention mechanism, convolutional layers of varying sizes, and Transformers. An adaptive loss function is introduced to guide model learning, addressing the limitations of traditional manually-designed loss functions and enhancing the depth of data mining. Extensive experiments demonstrate that MMIF-AMIN outperforms nine state-of-the-art MMIF methods, delivering superior results in both quantitative and qualitative analyses. Ablation experiments confirm the effectiveness of each component of the proposed method. Additionally, extending MMIF-AMIN to other image fusion tasks also achieves promising performance. MMIF-AMIN's code is available in the Supplementary Material.

1. Introduction

MMIF aims at integrating images from various medical imaging modalities to create high-quality medical images that are information-rich [1, 2, 3]. It plays a crucial role in aiding diagnosis and enhancing the effectiveness of medical clinical practices [4]. Medical images obtained from different modalities exhibit distinct imaging principles, image features and application contexts. The primary modalities in medical imaging encompass nuclear medicine imaging and magnetic resonance imaging (MRI). Nuclear medicine imaging comprises positron emission tomography (PET) and single-photon emission computed tomography (SPECT) [5]. These modalities operate by detecting metabolic activities or functional states using radioactive tracers, primarily for tumor identification. PET and SPECT, however, possess relatively low resolution, posing challenges in discerning small lesions or intricate structures [6]. In clinical settings, the amalgamation of MRI is often necessary for precise anatomical localization. MRI utilizes the inherent characteristics of organisms in a strong magnetic field to produce exceptionally detailed images, facilitating the visualization of anatomical features of soft tissues [7]. The primary goal of medical image fusion is to maintain the metabolic data from PET/SPECT scans, alongside the anatomical information and soft-tissue intricacies found in MRI images, while also conserving the distinct and complementary attributes of the original images to the greatest extent possible.

In recent years, medical image fusion techniques can be categorized into traditional methods and deep learning-based methods. Traditional methods typically involve spatial and frequency domain transformations, directly manipulating pixels for rapid fusion but often leading to image distortion [8, 9]. Frequency domain methods, utilizing

*Corresponding author
Email addresses: lt200136@email.swu.edu.com (Tao Luo), chxuwh@gmail.com (Weihua Xu)

Fourier or wavelet transforms, separate frequency information but are computationally intensive and lack spatial context integration, resulting in unnatural fusion outcomes [9]. Deep learning methods have attracted increasing attention due to the powerful feature extraction capabilities and advantages of convolutional neural networks (CNN). They have achieved remarkable performance in computer vision tasks such as image segmentation and object recognition [10, 11, 12].

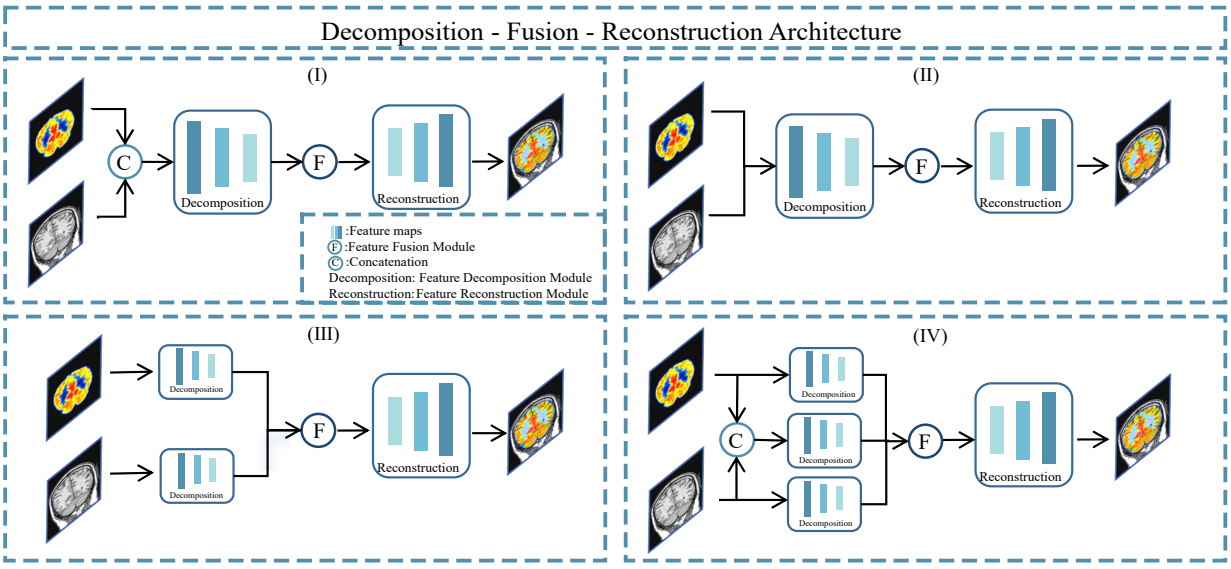

Figure 1: The architecture of the MMIF methods, Decomposition - Fusion - Reconstruction Architecture.

In multimodal image fusion research, an increasing number of studies have recently attempted to combine CNN and Transformer models to enhance image fusion performance [9, 13]. This approach aims to address the limitations of CNN in capturing contextual information and the challenges faced by Transformer in accurately capturing local information. The typical process for MMIF includes three main stages. These are decomposition, fusion, and reconstruction. The schematic representations of these processing architectures are illustrated in Figure 1. Architectures I and II incorporate a shared feature decomposition module, which may not effectively separate the distinctive features of each modality, such as U2Fusion and MATR [14, 8]. While Architecture III can capture the unique features of individual modalities, it overlooks the synergistic information present across modalities, such as MSPRN and CDDFuse [15, 16]. Our proposed Architecture IV is designed to extract both the distinctive features of individual modalities and the complementary information between multimodal images to a greater extent.

Due to the absence of a reference image for image fusion results, all deep learning-based MMIF methods resort to self-supervised techniques. The efficacy of self-supervised methods hinges on the formulation of the loss function, which is manually crafted in current MMIF approaches. Typically, these loss function parameters are tailored towards optimizing the fusion outcome, albeit at the expense of interpretability. Moreover, significant time and computational resources are typically expended in the quest for the optimal parameter configuration.

This paper introduces a novel method. The method aims to address the aforementioned issues. It does so by maximizing the retention of information from source images. Additionally, it acquires complementary information. This leads to optimal fusion outcomes. Single-modality image feature extraction is achieved using reversible neural networks to ensure lossless information transmission. MCFEM is designed with a Convolutional Block Attention Module (CBAM) to capture crucial information from different modalities [17]. By integrating CNN and Transformer [18] at various scales, context information and local details of complementary data are obtained to preserve essential complementary information. A data-driven loss function is constructed, where all parameters are data-dependent rather than manually set. This loss function incorporates structural-level feature information and regional-level details, combined with average gradient and entropy values from the source images.

In summary, the main contributions of this paper are as follows:

- A novel MMIF architecture is proposed to effectively extract the unique information and complementary features from multimodal images, thereby generating high-quality fused images. Specifically, IDN is employed to ensure the extraction of unique information. Furthermore, MCFEM is integrated to facilitate learning of diverse hierarchical features, thereby mitigating feature degradation issues during fusion.
- An adaptive loss function was developed, where the loss function is determined by characteristics of the source image rather than relying on manually set hyperparameters. Research shows that this adaptive loss function performs better than traditionally designed loss functions, thereby significantly reducing the demand for computational resources and enhancing the interpretability of the model.
- Comprehensive experiments on mainstream datasets show that this method outperforms the state-of-the-art (SOTA) methods. The performance of MMIF-AMIN was further validated through a generalization performance test, which demonstrated its superior performance on other multimodal medical or biological images.

2. Related work

Traditional medical image fusion methods fall into three main groups. These include spatial domain algorithms [19], frequency domain algorithms [20, 21], and other approaches [22]. Traditional methods for feature extraction and fusion rely heavily on manual design and the fusion results exhibit distortion.

The deep learning-based MMIF methods can effectively alleviate the issues caused by traditional approaches. Currently, deep learning-based methods can be mainly divided into two categories, CNN-based MMIF and hybrid model-based MMIF. The CNN-based networks include ResNet [15, 23], DenseNet [24] and other convolutional neural networks, which lack the capability for long-range modeling. In hybrid models, the most common type is the CNN-Transformer hybrid model [8, 9], which enables global modeling of images but requires substantial computational resources. Other examples include DWT-Invertible neural network hybrid models [25] and INN-Transformer hybrid models [16].

In recent years, due to the lossless information transmission capability and lightweight characteristics of invertible neural network (INN), they have been gradually applied in the field of computer vision. In the field of MMIF, researchers employ the INN method in two main ways. On the one hand, Integrating INN within the network, typically at the feature extraction or feature reconstruction stage. For instance, MMIF-INet [25] incorporates the INN block post Discrete Wavelet Transform (DWT), potentially leading to the loss of crucial information during feature extraction. On the other hand, Employing INN as the primary framework for single-modality feature extraction or fusion. For example, CDDFuse [16] utilizes the INN block solely on the processing branches of individual modalities, overlooking the significance of leveraging complementary information across modalities. While these approaches demonstrate notable fusion performance by leveraging the INN method differently, they still exhibit certain limitations, notably in neglecting the synergistic benefits of multi-modality information and applying INN subsequent to information loss.

3. The Proposed Method

3.1. Overview of the Framework

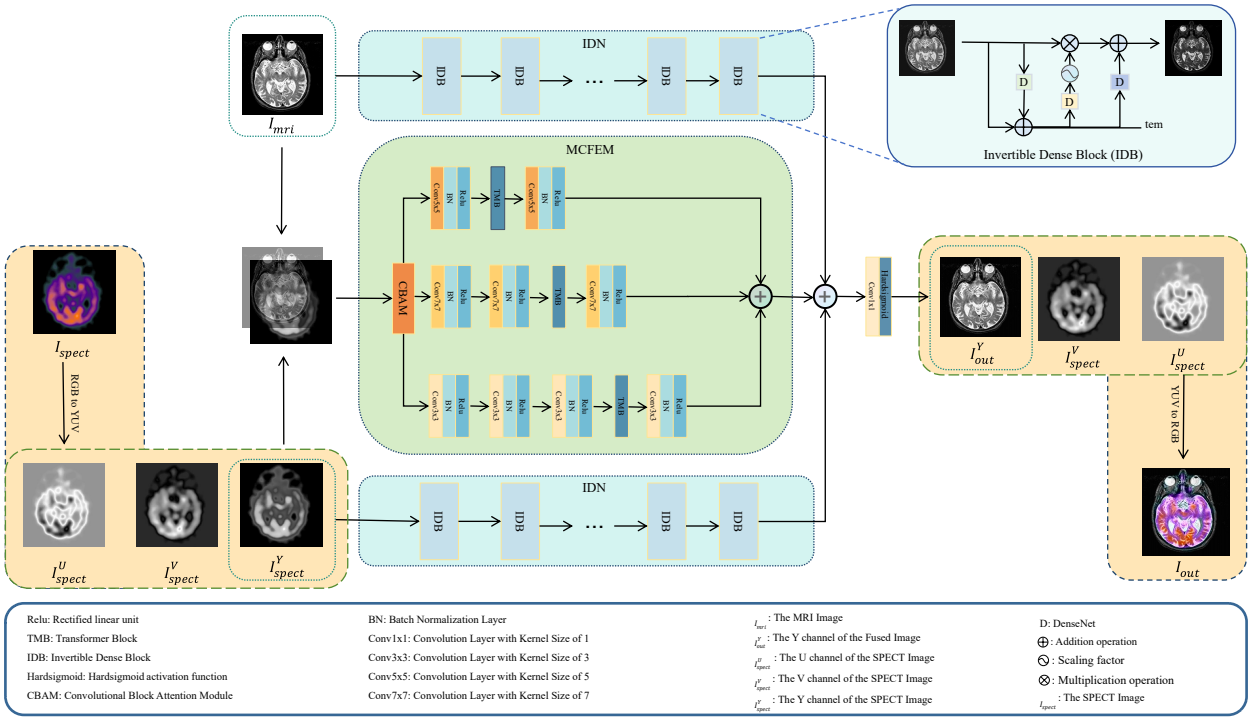

Figure 2: The overall network structure of the proposed MMIF-AMIN.

The Fusion model, as depicted in Figure 2, It comprises four main components. The first two are IDN modules used for lossless extraction of unique features from the two modal images. The third is a MCFEM, designed to capture complementary information. The fourth is a feature reconstruction module, consisting of 1x1 convolution and HardSigmoid. In medical image fusion tasks, RGB images are typically converted to YUV format, with the Y channels of multiple source images fused to address channel mismatch issues. 6 IDBs stacked within the IDN, aim to capture crucial information from source images, offering unique foundational features for subsequent fusion decisions, such as local contours and line directions. The general structure of the IDB, illustrated in Figure 3, primarily consists of a dense network and a scaling factor. The dense network facilitates direct transmission of shallow features to deeper layers through dense connections, mitigating the gradient vanishing problem. Additionally, it enables the extraction of semantic features at various levels, enhancing the acquisition of more sophisticated semantic features. The formula for this process is as follows:

$$\mathrm{R}_i = LeakyReLU\left(W_i * concat_{j=0}^{i-1}(\mathrm{R}_j) + b_i\right), \tag{1}$$

$$\mathrm{R}_{out} = W_5 \cdot concat_{j=0}^{4}\left(R_j\right) + b_5, \tag{2}$$

R_0 represents the input single-modal source image features, R_i denotes the output features of the i-th layer of the dense network where $i = (1, 2, 3, 4)$, LeakyRelu refers to the LeakyRelu activation function, W_i represents the weights of the convolutional kernel of the i-th layer, *concat* indicates the concatenation operation along the channel dimension, and b_i represents the bias of the i-th layer. The scaling factor plays a fundamental role in the architecture of invertible neural networks by adjusting feature maps while maintaining invertibility. When combined with an affine transformation in an affine coupling layer, it mitigates the need to store intermediate variables that arise from sequential calculations in conventional neural networks, thereby decreasing memory consumption[26]. Mathematically, it is represented as:

$$S_{out} = \exp(clamp \cdot 2 \cdot (Sigmoid(R_{out}) - 0.5)), \tag{3}$$

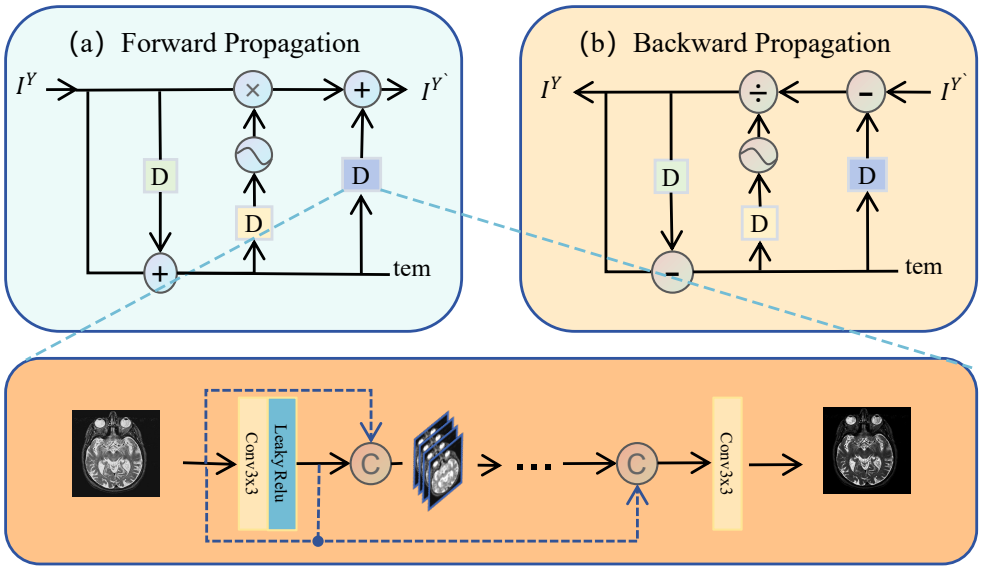

Figure 3: The specific structure of the invertible dense network. (a) represents the forward propagation process of the model, and (b) represents the backward propagation process of the model.

exp refers to the natural exponential function. R_{out} is the output of the dense network. clamp is a manually set parameter, with clamp is 2, which is used to limit the range of the scaling factor to avoid training instability caused by excessively large or small numerical values. Sigmoid is the Sigmoid activation function.

IDB enable lossless information transmission by utilizing identical parameters for both forward and backward propagation. Comprising a dense network and a scaling factor, they primarily execute reversible transformations. In Figure 3, "tem" is a temporary variable, during reverse propagation, intermediate variables are retrieved directly through inverse operations, obviating the need for storage. The incorporation of scaling factors mitigates issues such as gradient explosion or vanishing gradients. The integration of INN with dense networks facilitates comprehensive feature extraction from source images across multiple scales while maintaining information integrity. This approach not only enhances feature representation capabilities but also minimizes memory usage through the exploitation of reversibility.

3.2. Multi-scale Complementary Information Extraction

To leverage the synergistic information from multiple image sources effectively, MCFEM integrates a hybrid attention mechanism, convolution operation, and Transformer. The schematic representation of this module is illustrated in Figure 2. Our approach involves employing a multi-scale strategy to capture the complementary information that presented across diverse image sources [27, 28, 29]. The hybrid attention mechanism is designed to prioritize key regions by emulating the attentional patterns observed in human vision, thereby accentuating salient areas while suppressing redundant details [17]. By incorporating spatial and channel attention mechanisms, a multi-level weight distribution can be established to enhance spatial localization and feature semantics. The fusion of CNN and Transformer [18] architectures is intended to extract image features comprehensively from both global and local perspectives. Inspired by MATR[8], Our proposed hierarchical cascade architecture comprises a pre-positioned CNN for local feature extraction, a Transformer for capturing global semantics, and a post-positioned CNN for fine-tuning feature extraction. In this way, the effective utilization of complementary information is ensured.

3.2.1. Convolutional Block Attention Module

The Convolutional Block Attention Module (CBAM) combines channel attention and spatial attention in a cascaded manner [17]. This mechanism outperforms both spatial attention and channel attention mechanisms in enhancing semantic information of crucial channels and spatial details of respective regions. The specific structure of this

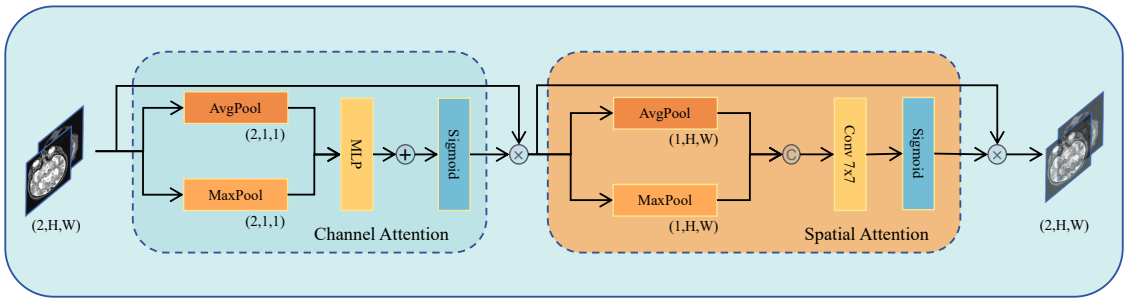

Figure 4: Overall network structure diagram of the Convolutional Block Attention Module.

mechanism is illustrated in Figure 4. Channel attention dynamically modifies the significance weights of individual channels based on global statistical data, as represented by the following formula:

$$M_c(X) = Sigmoid(MLP(AP(X)) + MLP(MP(X))), \tag{4}$$

X represents the Y component of the multi-modal images stitched along the channels. $Sigmoid$ refers to the sigmoid activation function. MLP stands for the multi-layer perceptron. AP and MP denote global average pooling and global max pooling, respectively. $M_c(X)$ represents the weight of channel attention.

Spatial attention focuses on the most discriminative spatial regions through local feature aggregation, and its formula is

$$M_s(X') = Sigmoid(Conv([AC(X'), MC(X')])), \tag{5}$$

X' refers to the dot product of $M_c(X)$ and X. Conv specifically denotes the 7x7 convolution operation. AC and MC represent the average pooling and max pooling in the channel dimension, respectively. $M_s(X)$ represents the weight of spatial attention.

Overall, the formula for CBAM is

$$CBAM(X) = M_s(M_c(X) \cdot X) \cdot (M_c(X) \cdot X), \tag{6}$$

X represents the Y component of the multi-modal images stitched along the channels. The cascaded structure achieves complementary enhancement in the channel and spatial dimensions, which improves the feature representation ability, and can significantly enhance the perception ability of key regions.

3.2.2. Transformer Module

Transformer unit (TMU) is a deep learning architecture based on the self-attention mechanism, which is mainly used to model and integrate the global dependencies in images and avoid the loss of global information. The specific architecture is shown in Figure 5. Specifically, the first step of TMU needs to go through Layer Normalization (LN). The layer serves to stabilize network training by addressing issues related to gradient vanishing and explosion. Additionally, the feature information is processed through a Multi-head Self-attention Mechanism (MSAM) to project it into multiple subspaces, extracting high-level semantic details from the source image. Subsequently, feature abstraction and enhancement are accomplished following the application of LN and a MLP. The corresponding formula is as follows:

$$TMU(X) = X + (MSAM(LN(X))) + \Big(MLP\Big(LN(X + (MSAM(LN(X))))\Big)\Big), \tag{7}$$

X is the processed result after multi-scale branch convolution. The TMB is composed of three TMUs. The first TMU focuses on capturing local context information, the second aims to establish cross-regional dependencies, and the third is designed to generate global semantic information. Through hierarchical feature extraction and long-range modeling, enhanced image quality can be achieved.

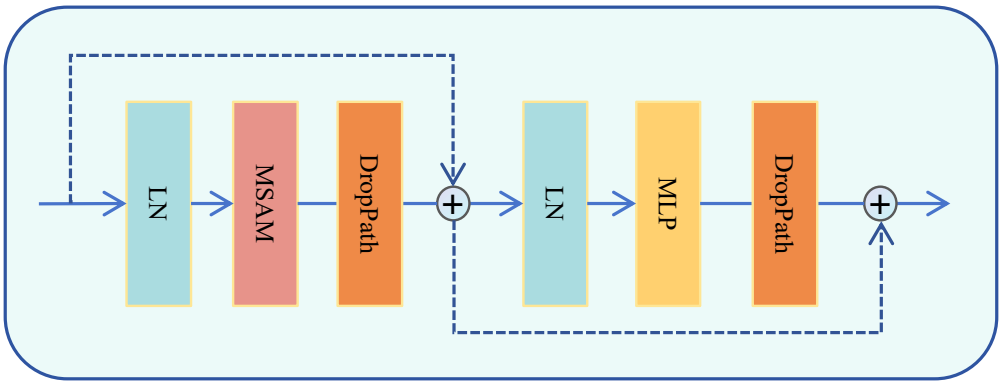

Figure 5: The specific structure diagram of the Transformer unit.

3.3. Adaptive Loss Function

The MMIF loss function typically integrates structural similarity loss, intensity loss, regional information loss, or other loss types, each modulated by hyperparametric weight combinations. In most MMIF methods [16, 9, 13], these combinations are determined through expert judgment or empirical findings and can be expressed as:

$$\mathcal{L}_{total} = \alpha\mathcal{L}_{ssim} + \beta\mathcal{L}_{other}, \tag{8}$$

$\mathcal{L}_{total}$ denotes the total loss function, $\alpha\mathcal{L}_{ssim}$ denotes the structural loss function, which is the structural similarity loss that most MMIF methods use, and is the loss function that MMIF methods set autonomously. The specific formula is as follows:

$$\alpha\mathcal{L}_{SSIM} = \alpha_1 \cdot (1 - SSIM(I_f, I_{mri})) + \alpha_2 \cdot (1 - SSIM(I_f, I_{spect})), \tag{9}$$

In the context of balancing structural losses across different modes, the parameter α is artificially set as $\{\alpha_1, \alpha_2\}$. The Structural Similarity Index (SSIM) evaluates the similarity between a fusion image and its source image, focusing on brightness, contrast and structure [30]. There exists a strong correlation between SSIM and the average gradient (AG) [31], where AG indicates image clarity. Generally, higher image quality corresponds to increased SSIM and AG values, demonstrating a positive relationship. Therefore, MMIF-AMIN uses the AG of the source image in place of α_1, α_2. The formula for AG is as follows:

$$AG = \frac{1}{|\mathcal{P}|} \sum_{p \in \mathcal{P}} \sqrt{(\Delta p_x)^2 + (\Delta p_y)^2}, \tag{10}$$

$\mathcal{P}$ represents the set of pixels, p represents a pixel point, Δp_x, Δp_y represents the horizontal difference, and represents the vertical difference.

Generally, $\beta\mathcal{L}_{other}$ is used to constrain either the local information or the global structure of the fused image. In MMIF-AMIN, we choose region mutual information (RMI) [32] loss as the constraint on local details, and its formula is

$$\beta\mathcal{L}_{RMI} = \beta_1 \cdot RMI(I_f, I_{mri}) + \beta_2 \cdot RMI(I_f, I_{spect}), \tag{11}$$

where $\beta \in \{\beta_1, \beta_2\}$, and it is typically adjusted artificially to equilibrate local information across different modes. RMI serves as a method to integrate discrepancies between images and source images at a local detail level. For aligned multimodal medical images, an increase in Entropy (EN) [33] corresponds to greater information content in regions of identical size. Therefore, instead of using manually designed β_1 and β_2, we leverage the EN of the source image to adjust the proportion of the multimodal image RMI. The formula for EN is as follows:

$$\mathrm{EN} = -\sum_{i=0}^{L} p_i \log_2 p_i, \tag{12}$$

where p_i is the probability density of the i-th gray level. L represents the number of gray levels, the value of L is 255.

The proposed MMIF-AMIN framework employs data-driven loss functions derived directly from source images, eschewing the need for manual design. Specifically, the loss function formula of MMIF-AMIN is

$$\mathcal{L}_{LOTAL} = \alpha\mathcal{L}_{SSIM} + \beta\mathcal{L}_{RMI}. \tag{13}$$

This approach mitigates errors associated with subjective design choices and enables collaborative optimization of multimodal data to better address clinical requirements.

4. Experiments

4.1. Experimental Settings

This section primarily introduces the experimental data sources and experimental equipment of MMIF-AMIN. Additionally, to demonstrate the superiority of MMIF-AMIN, 8 MMIF evaluation metrics and 9 MMIF methods are introduced.

4.1.1. Datasets

In the experiment, the images mainly used were from the public dataset provided by Harvard Medical School (`https://www.med.harvard.edu/AANLIB/home.html`), which contains brain disease images of various modalities such as MRI, PET and SPECT. A total of 357 pairs of MRI and SPECT images were collected, among which 337 pairs were used for the network training task and 20 pairs were used for network evaluation. During the training phase, data augmentation techniques were employed. Specifically, a pair of 256x256 images was cropped into 36 pairs of 120x120 images.

4.1.2. Implementation details

The experiment is conducted using the PyTorch framework on a machine equipped with an NVIDIA GeForce RTX 6000 GPU. A batch size of 1 is utilized, and the model is trained for 30 epochs. The Adam optimizer is employed with an initial learning rate of 0.0001. The TMU has 8 attention heads. Through data preprocessing and data augmentation, the training dataset contains 11,877 pairs of MRI and SPECT images.

4.1.3. Evaluation indicators

The primary goal of medical image fusion is to deliver detailed and clear information for diagnosis and treatment. To thoroughly assess the quality of fused images, eight widely used objective metrics are employed. These metrics include entropy (EN) [33], average gradient (AG) [31], mutual information (MI), visual information fidelity for fusion (VIFF) [34], Quality Assessment of Blended Features (QABF) [35], peak signal-to-noise ratio (PSNR), normalized mutual information (NMI) [36], and absolute feature measurement (AFM) [37]. The detailed information of most metrics can be found in [38].

4.1.4. Comparison methods

To evaluate the results of image fusion, we selected nine representative and state-of-the-art methods for comparative analysis, considering quantitative metrics, qualitative assessment, and fusion model size. FATFusion [9], M4FNet [39], MATR [8], MRPAN [23], EMFusion [40], U2Fusion [14], and LFDT [13] are medical image fusion approaches that integrate Transformer and CNN-based deep learning components. MMIF-INet [25] and CDDFuse [16] are medical image fusion methods built upon Invertible Neural Networks (INN) as the backbone. The codes of these nine methods are all publicly available, and all parameters are provided by their authors, thus ensuring the fairness of the comparison.

4.2. Result and Analysis

4.2.1. Qualitative analysis

Figure 6 presents the fusion results of nine MMIF methods. To better illustrate the fusion outcomes, two magnified close-up views are provided. The fused images from U2Fusion and M4FNet fail to preserve the brightness and contrast of the source images, exhibiting color distortion. MATR and EMFusion can effectively extract MRI image details, providing sufficient anatomical information, but with relatively low brightness. CDDFuse exhibits poor local detail extraction, leading to distortion, particularly in boundary regions, as evident from the apparent black spots within the red frame. FATFuse preserves structural information well but has limitations in extracting local details, resulting in the loss of local details in both the green frame and the high-brightness area within the red frame. In contrast, MMIF-INet, LFDT, and the proposed method (Ours) maintain the color and brightness of the source images while providing good soft-tissue detail information. Notably, the proposed method (Ours) offers more detailed information and clearer edges compared to the other approaches.

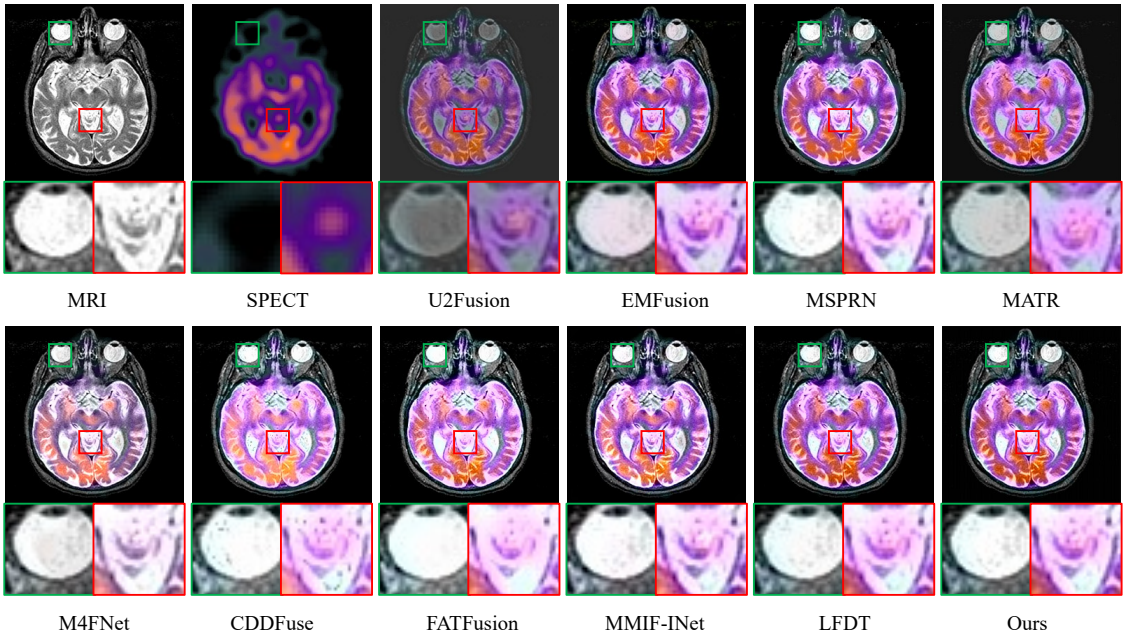

Figure 6: Qualitative illustration of various methods for merging MRI and SPECT images in image fusion tasks. The red and green boxes depict magnified local images at distinct positions to emphasize the qualitative impact of fusion.

4.2.2. Quantitative analysis

The proposed MMIF-AMIN demonstrates superior performance across multiple quantitative evaluation metrics compared to nine other MMIF methods. The scores presented in Table Table 1 represent the average of 20 pairs of test data for each indicator. MMIF-AMIN's exceptional rankings can be attributed to its novel architectural design. IDN effectively extracts the unique attributes of single-modal data, while MCFEM efficiently mines the complementary information between modalities. The fusion process in the reconstruction module generates a medical fusion image with rich information and a clear structure. MMIF-AMIN outperforms its competitors in seven out of the eight evaluation metrics and ranks third in the AG metric. This indicates that MMIF-AMIN has the best visual fidelity, the highest degree of information retention, clear edges, and the least distortion. In summary, the fusion results of MMIF-AMIN are superior to those of its competitors across multiple quantitative evaluation metrics, suggesting that it has the potential to provide effective assistance for clinical applications.

Methods	EN	AG	MI	VIFF	QABF	NMI	PSNR	AFM
U2Fusion [14]	4.1652	3.0428	1.8177	1.3270	0.3065	2.4463	24.4617	0.3897
EMFusion [40]	4.4384	5.0974	2.1411	1.6010	0.6910	2.5518	42.9036	0.6063
MRPAN [23]	4.3222	4.6784	2.8486	1.3580	0.5325	2.6798	40.9431	0.3525
MATR [8]	4.6947	5.1367	2.5867	1.7022	0.7047	2.7108	38.8409	0.6717
M4FNet [39]	4.6682	5.9750	2.1721	1.5304	0.7091	2.5232	39.0171	0.5496
CDDFuse [16]	4.7056	6.0683	2.1686	1.4452	0.6390	2.5221	33.0993	0.4448
FATFusion [9]	4.4087	**6.9410**	2.6694	1.8548	0.7344	2.8019	39.5931	0.7401
MMIF-INet [25]	4.7847	6.5529	2.1066	1.5517	0.7104	2.5041	38.3014	0.5618
LFDT [13]	4.6385	6.0377	2.6849	1.8063	0.7573	2.7355	49.2004	0.7275
Ours	**4.8858**	6.0719	**2.9264**	**1.9284**	**0.7636**	**2.9663**	**52.9264**	**0.7513**

Table 1: Quantitative evaluation results of different MMIF methods in MRI and SPECT image fusion tasks. (Bold: the best; Underline: the second best)

4.2.3. Parameter analysis

This section evaluates the proposed method's superiority by comparing the model parameters and FLOPs of nine MMIF methods. For fairness, the test data consists of a pair of 256x256 MRI and SPECT image. The large parameter count in LFDT [13], FATFusion [9], M4FNet [39] and CDDFuse [16] is primarily due to the Transformer module, while U2Fusion's parameter size is attributed to DenseNet. MMIF-INet [25] exhibits a high parameter count but low FLOPs, owing to numerous modules with 1x1 convolutional layers and a small feature map scale. MRPAN [23] rely heavily on convolutional operations, avoiding computationally intensive structures like Transformers. MATR [8] has the fewest parameters and FLOPs, utilizing minimal stacked Transformer and convolutional layers for medical image fusion. The MMIF-AMIN's model parameters and FLOPs are relatively small due to the adoption of the IRB module, which reduces the parameter count. Nevertheless, the large feature map size at each stage results in relatively high FLOPs.

Methods	Model size	FLOPs
U2Fusion [14]	2575.05K	86.44G
EMFusion [40]	583.68K	19.64G
MRPAN [23]	92.61K	18.00G
MATR [8]	**10.60K**	**1.95G**
M4FNet [39]	111.65K	13.92G
CDDFuse [16]	1249.28K	80.06G
FATFusion [9]	2736.13K	404.73G
MMIF-INet [25]	749.322K	7.08G
LFDT [13]	18327.552K	119.24G
Ours	76.47K	7.37G

Table 2: Comparison results of model size and FLOPs of different MMIF methods when processing images of the same size. (Bold: the best; Underline: the second best)

5. Extension to MRI-PET Fusion Task

To evaluate the generalization performance of MMIF-AMIN, the original trained model was directly tested on PET and MRI image pairs. Twenty image pairs were selected from the Harvard medical dataset for testing.

5.1. Qualitative analysis

Figure 7 illustrates the fusion of PET and MRI images using MMIF-AMIN alongside nine other MIF methods. U2Fusion and M4FNet suffer from significant distortion, mishandling detailed textures and producing images with dull colors. MRPAN [23], CDDFuse [16] and MMIF-INet [25] overly emphasize PET image content, resulting in a

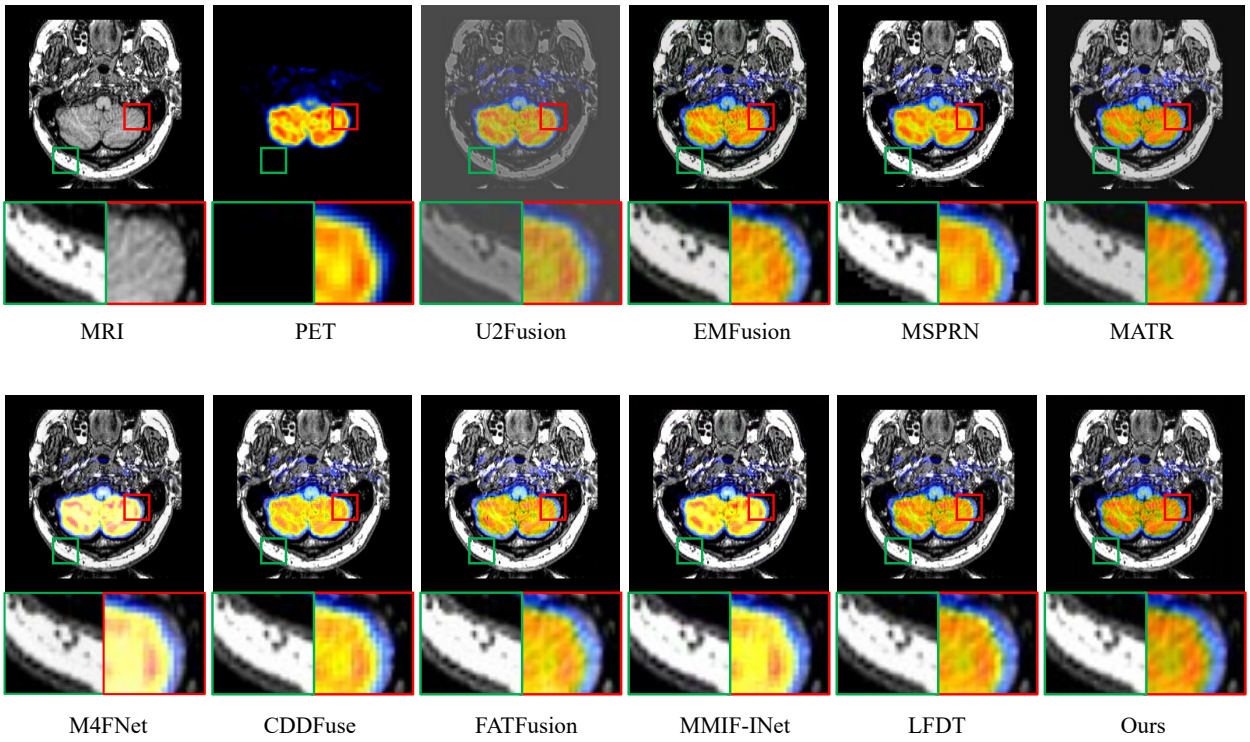

Figure 7: Qualitative illustrations of various methods in MRI and PET image fusion are presented. The red and green boxes depict magnified local views at distinct positions to emphasize the qualitative fusion effects.

loss of crucial texture details due to excessive focus on color information. EMFusion [40] and MATR [8] successfully capture detailed textures and display soft tissue information while preserving metabolic data, however, the soft tissue content appears too dark, compromising MRI brightness. FATFusion [9] maintains metabolic information well but struggles with extracting detailed textures, evident in the green frame's texture loss. LFDT [13] and our method effectively preserve image brightness and detail without color distortion, with our method outperforming LFDT [13] in maintaining textures. The results demonstrate that MMIF-AMIN effectively extracts unique and complementary features from source images and exhibits strong generalization capabilities.

5.2. Quantitative analysis

The proposed MMIF-AMIN method demonstrates superior performance compared to 9 other MMIF techniques across 6 evaluation metrics on both PET and MRI data. The decline in VIFF metric can be attributed to several factors. Firstly, the modal differences between the input data, as PET images are typically sparser and noisier than SPECT counterparts. This high noise or localized strong signals in PET data may lead to artifact diffusion in MMIF-AMIN, where noise is erroneously identified as valid signals. Secondly, the index characteristics play a role, as VIFF is based on human visual perception of "natural" images, whereas PET data presents unnatural local high brightness regions, which the VIFF metric may interpret as low-fidelity. However, when considering the holistic performance across multiple metrics, the proposed MMIF-AMIN method effectively extracts unique and complementary features from the source images, showcasing its strong generalization capability.

Methods	EN	AG	MI	VIFF	QABF	NMI	PSNR	AFM
U2Fusion [14]	4.6068	3.4933	1.6709	1.2884	0.1199	2.3504	16.7840	0.4528
EMFusion [40]	5.3518	9.4408	2.1521	1.0952	0.7385	2.4620	34.9229	0.6608
MRPAN [23]	4.7927	9.3640	2.7491	**1.4019**	0.6356	2.5935	31.4306	0.4129
MATR [8]	5.4165	8.3859	2.4127	1.0631	0.7247	2.5403	32.919	0.7327
M4FNet [39]	5.1575	9.7640	2.1736	1.1820	0.7106	2.4658	28.5000	0.4939
CDDFuse [16]	5.1620	10.2239	2.1052	1.1318	0.7020	2.4534	29.6226	0.5317
FATFusion [9]	5.2138	**11.4369**	2.5710	1.0544	0.7515	2.6127	33.1803	0.7554
MMIF-INet [25]	5.2209	10.9248	2.0945	1.1732	0.7353	2.4447	31.2328	0.5481
LFDT [13]	5.4432	10.4929	2.5247	1.0787	0.7740	2.5757	41.0523	0.7343
Our	**5.7079**	10.4260	**3.3050**	1.0515	**0.8023**	**2.9082**	**46.4487**	**0.8241**

Table 3: Quantitative evaluation results of different MMIF methods in MRI and PET image fusion tasks. (bold: the best; underlined: the second best)

6. Extension to Other Fusion Task

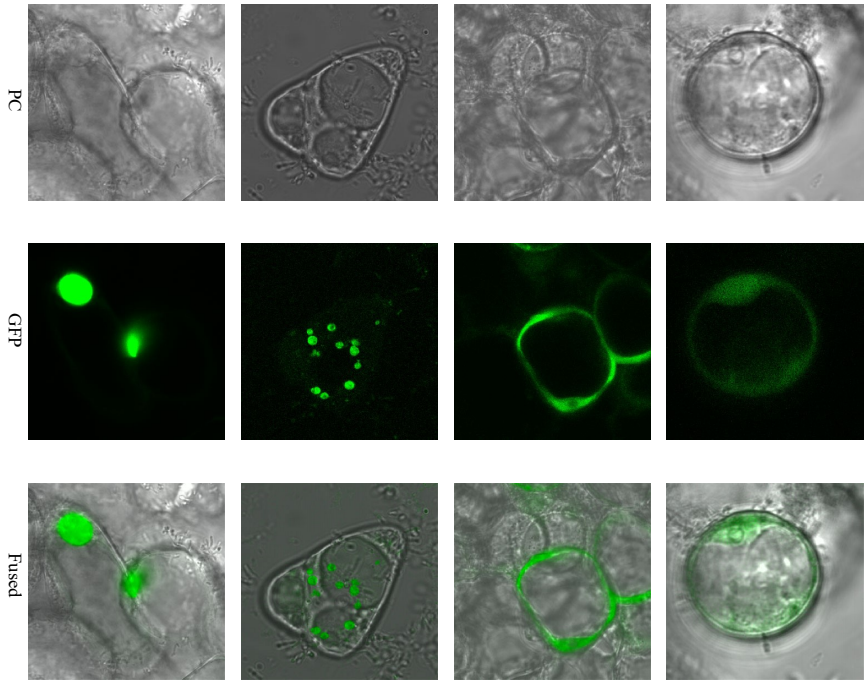

Figure 8: Qualitative illustrations of MMIF-AMIN on PC and GFP image fusion tasks are presented.

The proposed MMIF-AMIN method was further evaluated to assess its generalization capacity across diverse multimodal image fusion tasks. Specifically, the model was applied to fuse green fluorescent protein (GFP) and phase-contrast (PC) images, without any task-specific retraining of the model parameters, which remained identical to those used in the original experiments. This demonstration of the method's ability to generalize to new multimodal fusion scenarios without the need for additional training underscores its robustness and versatility. The parallels between the PC and GFP image fusion task and medical image fusion are noteworthy. GFP images, akin to SPECT and PET modalities, can convey specific information, while PC images, analogous to MRI, offer rich textural details. Consequently, the MMIF-AMIN framework is well-suited to address the PC and GFP image fusion challenge.

The presented Figure 8 showcases the ability of MMIF-AMIN to effectively extract textural details from PC images while preserving the color information from GFP images.

7. Ablation Studies

This section introduces the ablation experiments of MMIF-AMIN, focusing on two aspects: (1) The impact of the loss function design on experimental outcomes. (2) The validation of MMIF-AMIN's network structure effectiveness. The MMIF method necessitates a comprehensive evaluation from multiple assessment metrics. Accordingly, eight metrics are selected, specifically EN [33], AG [31], MI , VIFF [34], QABF [35], NMI [36], PSNR and AFM [37].

7.1. Effect of Network

Methods	EN	AG	MI	VIFF	QABF	NMI	PSNR	AFM
IDB_0	**5.3981**	4.1278	2.1091	1.4085	0.5515	2.4636	31.546	0.6327
IDB_1	4.8735	6.1684	2.8669	1.7896	0.7636	2.7365	50.2973	0.7638
IDB_2	4.5788	**6.2236**	2.8740	1.9120	**0.7645**	2.9355	51.4727	0.7665
IDB_3	4.9451	6.2086	2.9170	1.9254	0.7639	2.8583	51.9831	0.7501
IDB_4	4.9644	6.1372	2.9108	1.9258	0.7634	2.9319	52.1861	0.7500
IDB_5	4.7179	6.1127	2.8882	1.9225	0.7642	2.9130	51.3749	0.7671
TMU_0	4.0484	5.6471	**2.9538**	1.9181	0.7610	**3.0053**	46.4961	0.7671
TMU_1	4.6693	5.9277	2.7673	1.8577	0.7637	2.7741	51.7873	0.7634
TMU_2	4.7618	6.0095	2.8968	1.9189	0.7642	2.9501	**53.8832**	0.7592
CBAM_0	4.7337	6.0082	2.904	1.9151	0.7641	2.9429	52.2995	0.7619
MCFEM_0	3.9092	5.4724	2.8812	1.9003	0.7575	2.9912	42.0903	**0.7712**
all3x3	4.6226	5.3919	2.8328	1.8974	0.7581	2.8504	41.7649	0.7509
all5x5	4.6837	5.9265	2.9501	**1.9319**	0.7641	2.9680	49.0525	0.7669
all7x7	4.7054	5.8502	2.7738	1.8380	0.7633	2.7587	49.6535	0.7666
Ours	4.8858	6.0719	2.9264	1.9284	0.7636	2.9663	52.9264	0.7513

Table 4: Quantitative results of the ablation experiments for different modules in MMIF-AMIN,The numbering reflects the retained modules in different ablation experiments (such as IDB, TMB, etc.). For example, IDB_2 means that the ablation model employs 2 IDB modules. "all3x3" implies that all convolution kernels in MCFEM are of size 3×3. (bold: the best; underlined: the second best)

The efficacy of the MMIF-AMIN network architecture is examined through a two-pronged analysis. First, we evaluated the unique feature extraction module, specifically the selection of the number of IDBs, and its impact on the experimental outcomes. Second, we analyzed the MCFEM, to elucidate the influence of the convolution kernel size, the number of TMUs, and CBAM on the overall results.

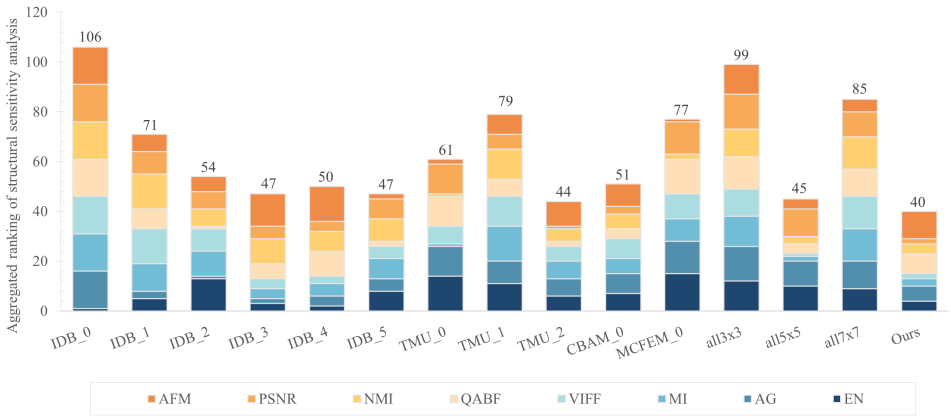

Figure 9: Ranking aggregation results of 8 evaluation indicators in the structural ablation experiment of MMIF-AMIN.

The proposed model employs IDN as the primary feature extraction module. The number of IDBs used can modulate the level of semantic information captured from the input image. Utilizing too few IDBs may limit the extraction of high-level semantic features, while an excessive number could lead to the overlooking of low-level features.

The complementary information extraction module focuses on the CBAM, TMU, and convolution kernel. As shown in Table 4 and Figure 9, the CBAM mechanism can effectively extract information from each modality, achieving a balance between modality specificity and complementarity. The multiple TMU layers, in essence, serve to progressively enhance the feature abstraction level and context modeling capability. Specifically, an insufficient number of stacked TMU layers may result in inadequate feature abstraction, thereby failing to capture complex global correlations. Conversely, an excessive number of stacked layers will lead to an increase in parameter scale and computational cost, which may further induce overfitting issues.

The MCFEM employs a hybrid utilization of convolution kernels with different sizes, enabling feature extraction at multiple granularity levels and constructing more abundant and deeper feature representations. This characteristic contributes to a more comprehensive description of various types of information in medical images. For instance, it can not only capture the overall location of lesion regions but also preserve their edge details. It is worth noting that large convolution kernels, which possess a larger receptive field, tend to focus more on global information, yet they are prone to losing local detailed information. In contrast, small convolution kernels, due to their limited receptive field, often fail to provide sufficient contextual information. Table 4 and Figure 9 results present the mean values and ranking statistics of the test image metrics, respectively. The comprehensive model demonstrates superior performance compared to the ablation variants.

7.2. Effect of Loss Function

Parameters	EN	AG	MI	VIFF	QABF	NMI	PSNR	AFM
{0.2,0.8,1,1}	**6.0835**	**6.8688**	2.4669	1.7239	0.691	2.5586	46.1612	0.6586
{0.4,0.6,1,1}	4.6661	<u>6.085</u>	2.8748	<u>1.9304</u>	0.7608	2.9083	47.8588	0.7472
{0.6,0.4,1,1}	4.5451	5.6861	**2.978**	1.9262	<u>0.7614</u>	**2.9932**	45.4515	0.7523
{0.8,0.2,1,1}	4.2907	5.7594	2.8452	1.9117	0.7606	2.9068	44.0993	**0.7652**
{1,1,0.2,0.8}	4.4061	6.0563	2.6025	1.8454	0.7446	2.7761	**53.4751**	0.7459
{1,1,0.4,0.6}	4.327	6.0112	2.9008	1.9269	<u>0.7614</u>	2.9266	46.471	<u>0.7629</u>
{1,1,0.6,0.4}	4.5784	5.9198	2.8907	**1.9305**	0.7595	2.9188	49.7649	0.7557
{1,1,0.8,0.2}	<u>6.0835</u>	6.8688	2.4893	1.746	0.7169	2.635	45.283	0.6752
Ours	4.8858	6.0719	<u>2.9264</u>	1.9284	**0.7636**	<u>2.9663</u>	<u>52.9264</u>	0.7513

Table 5: Quantitative results of MMIF-AMIN using loss functions with different weights,The sequence of parameters is $\{\alpha_1, \alpha_2, \beta_1, \beta_2\}$. (Bold: the best; Underline: the second best)

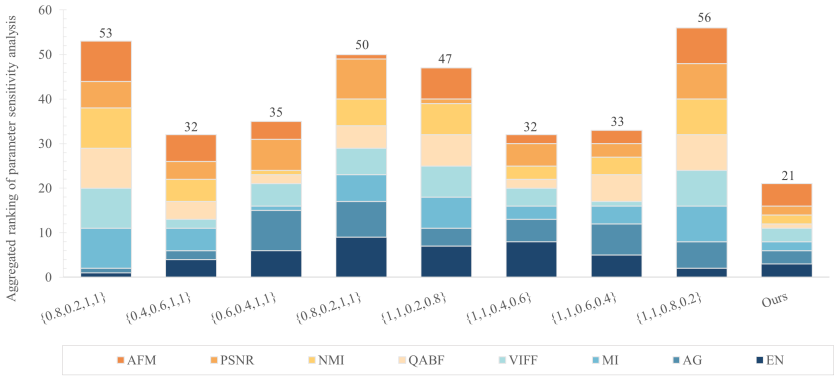

Figure 10: Ranking aggregation results of eight evaluation indicators in the parameter ablation experiment of MMIF-AMIN.

To assess the adaptive loss function's effectiveness, we evaluated eight manually designed training parameter combinations on SPECT and MRI images,the order of hyperparameter combinations is $\{\alpha_1, \alpha_2, \beta_1, \beta_2\}$. Table 5 presents average test set metrics, while Figure 10 ranks each parameter combination across various metrics. The data reveal that increasing the SSIM weight ratio between SPECT and MRI images results in a decrease in EN, AG and PSNR, whereas other metrics improve. Conversely, increasing the RMI weight ratio yields the opposite effect. Neither loss weight combination surpasses MMIF-AMIN. However, the comprehensive ranking shown in Figure 10 indicates that the adaptive loss function is overall superior to manually designed combinations. Therefore, the adaptive weights in the loss function can generate fused images of better quality.

8. Conclusion

This paper has presented a novel MMIF model, MMIF-AMIN, with a unique architecture. MMIF-AMIN has primarily utilized an IDN for lossless extraction of single-modality information and has realized the extraction of multi-modality and multi-scale complementary information through the MCFEM. Additionally, an adaptive loss function has been designed to overcome the limitations of traditional manual configuration of loss function weights, further explore the properties of source image data, and provide enhanced theoretical support for the interpretability of the model. Qualitative and quantitative results have demonstrated the model's excellent performance. Compared to nine other state-of-the-art methods, MMIF-AMIN has achieved the optimal comprehensive fusion effect. Moreover, when applied to MRI and PET multi-modality images, as well as GFP and PC multi-modality images, MMIF-AMIN has exhibited very good fusion performance. Ablation experiments have verified the effectiveness of the proposed approach, the relevant content is available in the supporting materials. In conclusion, MMIF-AMIN has had practical application value, including the potential to enhance subsequent tasks such as image detection and image segmentation.

References

[1] B. Huang, F. Yang, M. Yin, X. Mo, C. Zhong, A review of multimodal medical image fusion techniques, Computational and mathematical methods in medicine 2020 (1) (2020) 8279342.

[2] S. U. Khan, M. A. Khan, M. Azhar, F. Khan, Y. Lee, M. Javed, Multimodal medical image fusion towards future research: A review, Journal of King Saud University-Computer and Information Sciences 35 (8) (2023) 101733.

[3] S. Basu, S. Singhal, D. Singh, A systematic literature review on multimodal medical image fusion, Multimedia tools and applications 83 (6) (2024) 15845–15913.

[4] A. P. James, B. V. Dasarathy, Medical image fusion: A survey of the state of the art, Information fusion 19 (2014) 4–19.

[5] M. A. Azam, K. B. Khan, S. Salahuddin, E. Rehman, S. A. Khan, M. A. Khan, S. Kadry, A. H. Gandomi, A review on multimodal medical image fusion: Compendious analysis of medical modalities, multimodal databases, fusion techniques and quality metrics, Computers in biology and medicine 144 (2022) 105253.

[6] D. Shen, G. Wu, H.-I. Suk, Deep learning in medical image analysis, Annual review of biomedical engineering 19 (1) (2017) 221–248.

[7] F. Ritter, T. Boskamp, A. Homeyer, H. Laue, M. Schwier, F. Link, H.-O. Peitgen, Medical image analysis, IEEE pulse 2 (6) (2011) 60–70.

[8] W. Tang, F. He, Y. Liu, Y. Duan, Matr: Multimodal medical image fusion via multiscale adaptive transformer, IEEE Transactions on Image Processing 31 (2022) 5134–5149.
[9] W. Tang, F. He, Fatfusion: A functional–anatomical transformer for medical image fusion, Information Processing & Management 61 (4) (2024) 103687.
[10] S.-C. Huang, A. Pareek, M. Jensen, M. P. Lungren, S. Yeung, A. S. Chaudhari, Self-supervised learning for medical image classification: a systematic review and implementation guidelines, NPJ Digital Medicine 6 (1) (2023) 74.
[11] B. Rokh, A. Azarpeyvand, A. Khanteymoori, A comprehensive survey on model quantization for deep neural networks in image classification, ACM Transactions on Intelligent Systems and Technology 14 (6) (2023) 1–50.
[12] R. Archana, P. S. E. Jeevaraj, Deep learning models for digital image processing: a review, Artificial Intelligence Review 57 (1) (2024) 33.
[13] B. Yang, Z. Jiang, D. Pan, H. Yu, G. Gui, W. Gui, Lfdt-fusion: a latent feature-guided diffusion transformer model for general image fusion, Information Fusion 113 (2025) 102639.
[14] H. Xu, J. Ma, J. Jiang, X. Guo, H. Ling, U2fusion: A unified unsupervised image fusion network, IEEE transactions on pattern analysis and machine intelligence 44 (1) (2020) 502–518.
[15] H. Jung, Y. Kim, H. Jang, N. Ha, K. Sohn, Unsupervised deep image fusion with structure tensor representations, IEEE Transactions on Image Processing 29 (2020) 3845–3858.
[16] Z. Zhao, H. Bai, J. Zhang, Y. Zhang, S. Xu, Z. Lin, R. Timofte, L. V. Gool, Cddfuse: Correlation-driven dual-branch feature decomposition for multi-modality image fusion, 2023 IEEE/CVF Conference on Computer Vision and Pattern Recognition (CVPR) (2023) 5906–5916.
URL https://api.semanticscholar.org/CorpusID:254043982
[17] S. Woo, J. Park, J. Y. Lee, I. S. Kweon, Cbam: Convolutional block attention module, Springer, Cham (2018).
[18] A. Dosovitskiy, L. Beyer, A. Kolesnikov, D. Weissenborn, N. Houlsby, An image is worth 16x16 words: Transformers for image recognition at scale (2020).
[19] Z. Cui, G. Zhang, J. Wu, Medical image fusion based on wavelet transform and independent component analysis, in: 2009 International Joint Conference on Artificial Intelligence, IEEE, 2009, pp. 480–483.
[20] R. Singh, R. Srivastava, O. Prakash, A. Khare, Multimodal medical image fusion in dual tree complex wavelet transform domain using maximum and average fusion rules, Journal of Medical Imaging and Health Informatics 2 (2) (2012) 168–173.
[21] V. Bhavana, H. Krishnappa, Multi-modality medical image fusion using discrete wavelet transform, Procedia Computer Science 70 (2015) 625–631.
[22] W. Kong, Y. Lei, H. Zhao, Adaptive fusion method of visible light and infrared images based on non-subsampled shearlet transform and fast non-negative matrix factorization, Infrared Physics & Technology 67 (2014) 161–172.
[23] J. Fu, W. Li, J. Du, Y. Huang, A multiscale residual pyramid attention network for medical image fusion, Biomedical Signal Processing and Control 66 (2021) 102488.
[24] S. Ye, T. Wang, M. Ding, X. Zhang, F-darts: Foveated differentiable architecture search based multimodal medical image fusion, IEEE Transactions on Medical Imaging 42 (11) (2023) 3348–3361. doi:10.1109/TMI.2023.3283517.
[25] D. He, W. Li, G. Wang, Y. Huang, S. Liu, Mmif-inet: Multimodal medical image fusion by invertible network, Information Fusion 114 (2025) 102666.
[26] L. Dinh, D. Krueger, Y. Bengio, Nice: Non-linear independent components estimation, arXiv e-prints (2014).
[27] X. Li, W. Zhang, Q. Ding, Deep learning-based remaining useful life estimation of bearings using multi-scale feature extraction, Reliability engineering & system safety 182 (2019) 208–218.
[28] K. Zhou, M. Zhang, H. Wang, J. Tan, Ship detection in sar images based on multi-scale feature extraction and adaptive feature fusion, Remote Sensing 14 (3) (2022) 755.
[29] S. Lu, Y. Ding, M. Liu, Z. Yin, L. Yin, W. Zheng, Multiscale feature extraction and fusion of image and text in vqa, International Journal of Computational Intelligence Systems 16 (1) (2023) 54.
[30] Z. Wang, A. C. Bovik, H. R. Sheikh, E. P. Simoncelli, Image quality assessment: from error visibility to structural similarity, IEEE transactions on image processing 13 (4) (2004) 600–612.
[31] A. M. Eskicioglu, P. S. Fisher, Image quality measures and their performance, IEEE Transactions on communications 43 (12) (2002) 2959–2965.
[32] S. Zhao, Y. Wang, Z. Yang, D. Cai, Region mutual information loss for semantic segmentation, Advances in Neural Information Processing Systems 32 (2019).
[33] J. W. Roberts, J. A. Van Aardt, F. B. Ahmed, Assessment of image fusion procedures using entropy, image quality, and multispectral classification, Journal of Applied Remote Sensing 2 (1) (2008) 023522.
[34] Y. Han, Y. Cai, Y. Cao, X. Xu, A new image fusion performance metric based on visual information fidelity, Information fusion 14 (2) (2013) 127–135.
[35] C. S. Xydeas, V. Petrovic, Objective image fusion performance measure, Electronics letters 36 (4) (2000) 308–309.
[36] M. Hossny, S. Nahavandi, D. Creighton, Comments on 'information measure for performance of image fusion', Electronics letters 44 (18) (2008) 1066–1067.
[37] J. Zhao, R. Laganiere, Z. Liu, Performance assessment of combinative pixel-level image fusion based on an absolute feature measurement, Int. J. Innov. Comput. Inf. Control 3 (6) (2007) 1433–1447.
[38] J. Ma, Y. Ma, C. Li, Infrared and visible image fusion methods and applications: A survey, Information fusion 45 (2019) 153–178.
[39] Z. Ding, H. Li, Y. Guo, D. Zhou, Y. Liu, S. Xie, M4fnet: Multimodal medical image fusion network via multi-receptive-field and multi-scale feature integration, Computers in Biology and Medicine 159 (2023) 106923. doi:https://doi.org/10.1016/j.compbiomed.2023.106923.
URL https://www.sciencedirect.com/science/article/pii/S0010482523003888
[40] H. Xu, J. Ma, Emfusion: An unsupervised enhanced medical image fusion network, Information Fusion 76 (2021) 177–186.